

REPORT DOCUMENTATION PAGE			<i>Form Approved</i> OMB No. 0704-0188		
Public reporting burden for this collection of information is estimated to average 1 hour per response, including the time for reviewing instructions, searching existing data sources, gathering and maintaining the data needed, and completing and reviewing this collection of information. Send comments regarding this burden estimate or any other aspect of this collection of information, including suggestions for reducing this burden to Department of Defense, Washington Headquarters Services, Directorate for Information Operations and Reports (0704-0188), 1215 Jefferson Davis Highway, Suite 1204, Arlington, VA 22202-4302. Respondents should be aware that notwithstanding any other provision of law, no person shall be subject to any penalty for failing to comply with a collection of information if it does not display a currently valid OMB control number. PLEASE DO NOT RETURN YOUR FORM TO THE ABOVE ADDRESS.					
1. REPORT DATE (DD-MM-YYYY) 13-06-2007		2. REPORT TYPE Technical Paper		3. DATES COVERED (From - To)	
4. TITLE AND SUBTITLE Dark Core Analysis of Coaxial Injectors at Sub-, Near-, and Supercritical Pressures in a Transverse Acoustic Field (Postprint)			5a. CONTRACT NUMBER		
			5b. GRANT NUMBER		
			5c. PROGRAM ELEMENT NUMBER		
6. AUTHOR(S) Ivett A. Leyva & Douglas Talley (AFRL/PRSA); Bruce Chehroudi (ERC)			5d. PROJECT NUMBER		
			5e. TASK NUMBER 23080533		
			5f. WORK UNIT NUMBER		
7. PERFORMING ORGANIZATION NAME(S) AND ADDRESS(ES) Air Force Research Laboratory (AFMC) AFRL/PRSA 10 E. Saturn Blvd. Edwards AFB CA 93524-7680			8. PERFORMING ORGANIZATION REPORT NUMBER AFRL-PR-ED-TP-2007-327		
9. SPONSORING / MONITORING AGENCY NAME(S) AND ADDRESS(ES) Air Force Research Laboratory (AFMC) AFRL/PRS 5 Pollux Drive Edwards AFB CA 93524-7048			10. SPONSOR/MONITOR'S ACRONYM(S)		
			11. SPONSOR/MONITOR'S NUMBER(S) AFRL-PR-ED-TP-2007-327		
12. DISTRIBUTION / AVAILABILITY STATEMENT Approved for public release; distribution unlimited (PA #07238A).					
13. SUPPLEMENTARY NOTES Presented at the 43 rd AIAA/ASME/SAE/ASEE Joint Propulsion Conference, Cincinnati, OH, 8-11 July 2007.					
14. ABSTRACT <p>An experimental study on the effects of an externally-imposed transverse acoustic field in a N₂ shear coaxial jets at sub-, near-, and supercritical pressures is presented. Such fields and their interaction with the jets (i.e., breakup, mixing, etc.) are believed to play a critical role during combustion instabilities in liquid rocket engines. The shear coaxial injector used here is similar to those used in cryogenic liquid rockets. By using N₂ as the working fluid, the chemistry effects on combustion instability are separated from the effects of a transverse acoustic field on coaxial jets. Furthermore, through this choice, ambiguities associated with composition dependence on mixtures critical properties are eliminated. The acoustic field is generated by a piezo-siren and the first resonant frequency is ~3kHz. The pressures in the chamber range from 215-716 psia to span subcritical to supercritical pressures. The outer to inner jet velocity ratio varies from ~1.2 to 23 and the momentum flux ratio (MR) varies from ~0.2 to 23. These ratios are mainly varied by changing the temperature and flow rates of the outer jet. At least 2000 backlit images were taken at 41kHz for each run. The main metric investigated is the length of the dark, or inner jet, core. This length is related to the mixing processes in a coaxial jet. The shorter the core length the faster the mixing occurs. Both the axial and the total, or curved, dark core lengths are studied. For momentum flux ratios ~1<MR<~4 the differences in the axial and curved dark core lengths between acoustics on and off are statistically significant, which means acoustics do shorten the core for this range. For subcritical pressures the MR range where the jet is shortened is larger. Preliminary results on the frequency analysis of the dark core lengths and width is also presented.</p>					
15. SUBJECT TERMS					
16. SECURITY CLASSIFICATION OF:			17. LIMITATION OF ABSTRACT	18. NUMBER OF PAGES	19a. NAME OF RESPONSIBLE PERSON
a. REPORT	b. ABSTRACT	c. THIS PAGE			19b. TELEPHONE NUMBER <i>(include area code)</i>
Unclassified	Unclassified	Unclassified	SAR	19	N/A

Dark core analysis of coaxial injectors at sub-, near-, and supercritical pressures in a transverse acoustic field

Ivett A. Leyva¹, Bruce Chehroudi² and Douglas Talley³
Air Force Research Laboratory, Edwards AFB, CA 93524

An experimental study on the effects of an externally-imposed transverse acoustic field in a N₂ shear coaxial jet at sub-, near-, and supercritical pressures is presented. Such fields and their interaction with the jet (i.e., breakup, mixing, etc.) are believed to play a critical role during combustion instabilities in liquid rocket engines. The shear coaxial injector used here is similar to those used in cryogenic liquid rockets. By using N₂ as the working fluid, the chemistry effects on combustion instability are separated from the effects of a transverse acoustic field on coaxial jets. Furthermore, through this choice, ambiguities associated with composition dependence on mixture critical properties are eliminated. The acoustic field is generated by a piezo-siren and the resonant frequency studied is ~3kHz. The pressures in the chamber range from 1.5-4.9 MPa to span subcritical to supercritical pressures. The outer to inner jet velocity ratio varies from ~1.2 to 23 and the momentum flux ratio (MR) varies from ~0.2 to 23. These ratios are mainly varied by changing the temperature and flow rates of the outer jet. At least 2000 backlit images were taken at 41kHz for each run. The main metric investigated is the length of the dark, or inner jet, core. This length is related to the mixing processes in a coaxial jet. The shorter the core length the faster the mixing occurs. Both the axial and the total, or curved, dark core lengths are studied. For momentum flux ratios $1 < MR < 4$ the differences in the axial and curved dark core lengths between acoustics on and off are statistically significant, which means acoustics do shorten the core for this range. For subcritical pressures the MR range where the jet is shortened is larger. Preliminary results on the frequency analysis of the dark core lengths and width is also presented.

Nomenclature

A	= constant
D	= diameter with subscripts
LRE	= liquid rocket engine
HE	= heat exchanger
L	= axial dark core length
L_t	= total or curved dark core length
MR	= outer to inner jet momentum flux ratio
n	= exponent for MR
P	= pressure
R	= radius with subscripts
T	= temperature
VR	= outer to inner jet velocity ratio

¹ Sr. Aerospace Engineer, AFRL/PRSA, Edwards AFB, CA 93524, AIAA Member.

² Principal Scientist, ERC Inc., AFRL, Edwards AFB, CA 93524, AIAA Member.

³ Sr. Aerospace Engineer, AFRL/PRSA, Edwards AFB, CA 93524, AIAA Member.

I. Introduction

THIS study is conducted with two overarching objectives in mind. The first objective is to understand the effects of transitioning from subcritical to supercritical pressure on a coaxial injector's jet characteristics such as mixing, atomization and breakup. This is because as liquid rockets engines (LRE's) have evolved into higher specific impulse designs, the chamber pressures have simultaneously increased reaching supercritical values for some propellants. The Space Shuttle Main Engine (SSME) and the Vulcan engine for the Ariane 5 launch vehicles are examples of LRE's designed to operate above the critical pressures of each propellant individually. We choose to study a coaxial injector since this design has proven effective for LRE's. In a typical coaxial injector for an LOX/LH2 engine, the oxygen is injected at subcritical temperatures in the center jet while the hydrogen is injected at supercritical temperatures, after being used as a coolant for the engine nozzle, in the coaxial jet. A typical velocity ratio between the outer and inner jets is about 10^1 . For these flows, as pointed out by previous researchers¹, the mixture no longer has a singular critical point but rather critical mixing lines that define its thermodynamic state. Therefore, a phase-diagram becomes necessary when studying mixtures that are at supercritical pressures with respect to their individual propellants. Because of the added complexity introduced when working with mixtures, N_2 is used as the sole working fluid.

The second objective is related to a problem that has been encountered since the late 1930's in LRE's, namely combustion instability². Of the different types of instabilities, high frequency or acoustic instabilities are the most destructive to an engine. The damage can range from minor to catastrophic failure of an engine³. While a comprehensive understanding of what triggers these instabilities and how they evolve is still underway, a few things seem to be agreed upon. These instabilities are the result of coupling between the chamber acoustic modes and the injector fluid processes such as propellant injection, atomization, droplet vaporization, mixing and heat release from combustion⁴. Of the different high-frequency acoustic modes, tangential modes (in the case of cylindrical chambers) seem to be the most damaging in rocket engines⁵⁻⁶. The equivalent of this mode in a rectangular chamber is a transverse mode. In the present study the coaxial jet with cryogenic N_2 is installed in a rectangular chamber. We excite this jet with a piezo-siren that produces high amplitude (max ~ 184 db) pressure oscillations and sets up a transverse standing acoustic field. The second objective is then to study the effects of the acoustics on the jet. This is done mostly by measuring the jet's dark core length (indicative of mixing efficiency) and its standard deviation as the outer-to-inner jet momentum flux ratio, MR, the outer-to-inner jet velocity ratio, VR, and the chamber pressure are varied. By doing the experiments with cryogenic N_2 , the aim is to study the sub-process of acoustic interaction with the jet in isolation from the heat release created by the combustion process. In this sense, these cryogenic cold flow experiments at high pressure can be viewed as an intermediate step between atmospheric water cold flow experiments and fully reacting experiments. The data gathered in this study (with and without the imposed acoustic field) also serves as a first step in validating CFD codes aimed to tackle combustion at supercritical pressure.

Previous studies done at the same facility at AFRL reported preliminary findings on the effects of a transverse acoustic field on a coaxial jet going from subcritical to supercritical pressures⁷⁻⁸. The current study is in part an extension of that work. The main differences are, 1) the ranges of MR and VR are larger in this study, 2) each data set now consists of at least 2000 images taken at a minimum sampling frequency of 41kHz (vs. 30 images taken at 10Hz), 3) introduction of the curved or total dark core length to look in more detail to the effects on mixing from acoustics, 4) different definitions and smoothing techniques applied for computing the dark core length are compared, and 5) a preliminary frequency analysis of the dark core length is given. With these enhancements, we have more confidence in the statistics of the dark core length and the conclusions drawn from these measurements.

II. Experimental Setup

The facility used for this study is the Cryogenic Supercritical Laboratory (EC-4) at the Air Force Research Laboratory (AFRL) at Edwards Air Force Base, CA. An overview of the facility is shown in Fig. 1. This facility has been extensively described in previous references⁷⁻⁸. Gaseous N_2 is used to supply the inner and outer jet flows and to pressurize the chamber. It is obtained from the main supply line to the lab. The outer and inner jets are cooled by three heat exchangers (HE's). The coolant is liquid nitrogen obtained from a cryogenic tank. One heat exchanger cools the inner jet and the other two cool the outer jet. The temperature (T) of the two jets is controlled by adjusting the flow rate of liquid nitrogen through the HE's. The mass flow rate through the inner and outer jets is measured, before they are cooled, with Porter mass flow meters (122 and 123-DKASVDAA). It was found that it is much easier to measure the flow rates at ambient rather than at cryogenic temperatures. The chamber pressure is measured

with a Stellar 1500 transducer. To keep the amplitude of the acoustic oscillations to a maximum near the jet, an inner chamber was created (Fig. 1). The inner chamber has nominal height of 6.6cm, width 7.6cm and depth 1.3cm. Details for the coaxial injector used are shown in Fig. 2. The inner diameter of the inner jet, D_1 , is 0.51 mm. The outer jet has an inner diameter, D_2 , of 1.59 mm and outer diameter, D_3 , of 2.42 mm. The length to inside diameter ratio is 100 for the inner jet and 67 for the outer jet (taking as reference the mean width of the annular passage, or hydraulic diameter). There is a small bias of about 8% of the mean gap width. As can be seen from the same figure, the inner jet is recessed by 0.3 mm from the outer jet.

The temperature of the jets is measured with a type E thermocouple which has a bead diameter of 0.1mm. The accuracy of this thermocouple was checked with an RTD and found to be $\pm 1K$. This thermocouple is traversed across the outer and inner jets to obtain a reading as close as possible to the injector exit plane (also seen in Fig. 1). The radial profiles of the temperature were taken at intervals of 0.1mm, or 0.05mm if the temperature varied significantly. The average distance from the exit plane, denoted H in Fig. 2 is $\sim 0.3mm$. Properties such as density, viscosity, and surface tension are computed from the measured flow rates, chamber pressure and jet temperature, using NIST's REFPROP⁹. From this, the Re , We , VR and MR for a given condition can be computed.

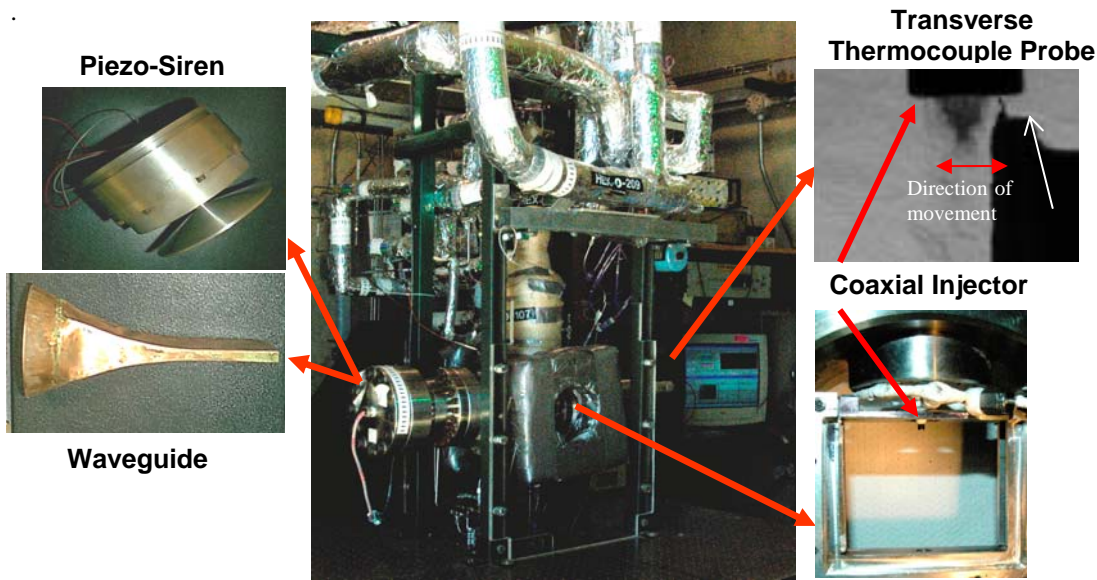


Figure 1. Overview of the Supercritical Flow Facility, EC-4 at AFRL/Edwards used for this study

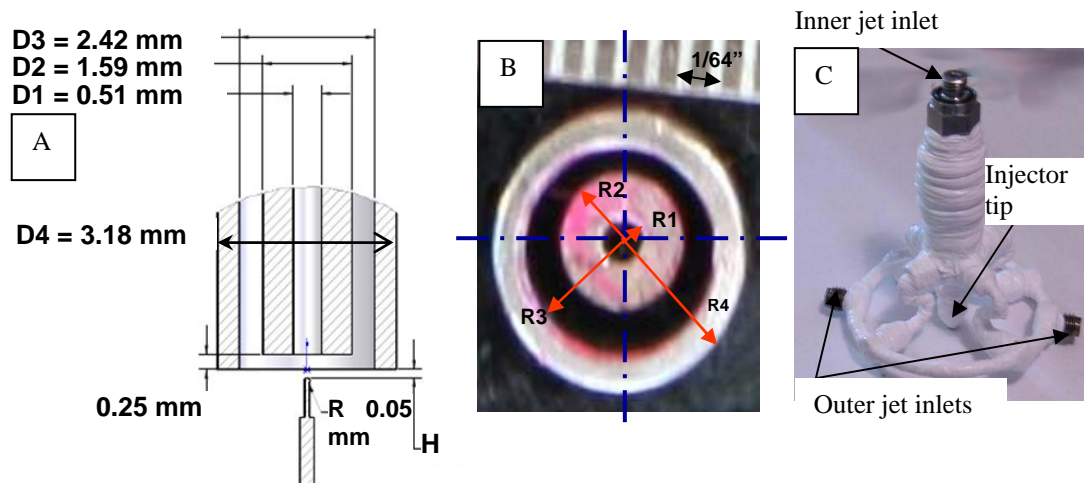


Figure 2. Details on the coaxial injector used for the present study

The jet is visualized by taking backlit images using a Phantom 7.1 CMOS camera. The images have 128x256 pixels, and each pixel represents an area of about 0.08mmx0.08mm. The framing rate is 41kHz. The exposure time varies from 7-9 μ s. The jet is backlit using a Newport variable power arc lamp set at 300W. The acoustic waves are generated using a piezo-siren custom-designed for AFRL by Hersh Acoustical Engineering, Inc. (Fig.1). A piezo-ceramic element is externally excited with a sinusoidal wave at the desired driving frequency for the system. This frequency is chosen by manually varying the frequency on a signal generator until the highest amplitudes for the pressure waves are obtained. This signal is amplified and then fed to the piezo-siren. The movement of the piezo element is transmitted to the aluminum cone attached to it, and the cone then produces acoustic waves. To accommodate for the rectangular chamber a waveguide with a catenary contour is used to guide the waves from a circular cross-section to a rectangular cross-section (also shown in Fig.1). The sound pressure levels (SPL) in the inner chamber range from 161 dB to 171 dB at for the first two resonance frequencies (~3.0 kHz and ~5.2 kHz). In this study only the first resonant frequency is studied.

IV. Results and Discussion

A total of 44 runs were completed spanning chamber pressures from 1.5 to 4.9 MPa. The runs are divided into subcritical, nearcritical and supercritical pressures. For reference, for N₂, the critical P is 3.40 MPa, and the critical T is 126.26 K. Within each pressure range, there is a subset of high T outer jet and a subset of low T outer jet. Details of the test conditions are presented in the Appendix. Table 1 summarizes the range of conditions for each chamber pressure. Since the major parameter of interest for this study is the core length, a graphical representation of the definitions for the axial and curved or total length is shown in Fig. 3 (Pchamber =1.49 MPa, VR=7.49, MR=2.64 and the acoustic field is on).

Table 1. Summary of range of conditions for each pressure range

Mean Chamber pressure, P (MPa)	Outer to inner jet Velocity ratio, VR	Outer to inner jet momentum flux ratio, MR	Range of inner jet temperature (K)	Nominal inner jet mass flow rate (mg/s)	Range of outer jet temperature (K)
1.48	1.9 – 22.6	0.2 – 23.3	109 – 110	280	144 – 195
3.55	1.3 – 5.9	0.3 – 9.1	123 – 132	289	138 – 195
4.93	1.2 – 4.8	0.3 – 10.3	132 – 147	294	150 – 195

The first observation in the unprocessed image (leftmost image) is that the inner jet, which is colder and denser than the outer jet, appears darker in the backlit image. It is the length of this denser core, before its first break, that is called the dark core length. Historically, people have defined the dark core length or intact length as the projection of the core in the axial direction (y) as shown in Fig. 3. In this study, this is called the axial dark core length. There are many valid ways to define this length. One only has to be cautious that the method chosen agrees with the intuitive length judged by the naked eye. Several methods to compute the axial dark core length were analyzed by this group. In general, to arrive at a length from raw images, a series of steps need to be taken. The first step is to convert the grayscale images to black and white (b&w) images. This is typically done by choosing a threshold value of pixel intensity below which all pixels are set to black and above which all pixels is set to white. Choosing an adequate threshold is the first logic rule that is implemented when automating the length measurements. After converting the image to b&w one has to define the first break in the jet. This would be the second logic rule that is implemented. Finally, if a total or curved length is desired (Fig 3), then one needs to decide if the curve needs to be smoothed before the final curve measurement is made.

In the present case, the raw images taken with the Phantom camera are first converted to a multi-page tiff format and then analyzed using Matlab. Matlab is chosen over other image processing programs such as ImagePro because it is faster. The raw images are converted, or thresholded, to a b&w image using Matlab’s subroutine “im2bw” (Fig. 3B). The threshold level is determined using Matlab subroutine “graythresh”. This subroutine uses Otsu’s method¹⁰ and it is based on the zeroth and first cumulative moments of the gray-level histogram. In previous studies from this lab⁷⁻⁸ the threshold was found by constructing a histogram of the image and defining the threshold value as the pixel

intensity where the slope of histogram is equal to $1/e$. The current method to define a threshold is preferred due to its robustness. Once a b&w image is obtained, the axial length of the jet is determined by drawing a contour around the image (using Matlab subroutine “imcontour”) and measuring the y coordinate of the longest contour that is attached to the injector as shown in Fig. 3. Other ways to define the length include measuring the location when the standard deviation of the pixel intensity of a row is zero. This method tends to overpredict the length when the jet break is not clean and there are dark lumps clustered around the jet breakup region. For clean breaks both methods agree very well. It is noteworthy to say that even though the magnitudes might be different with the different definitions for the lengths, the trends of the axial dark core length and its standard deviation with respect to MR and VR are preserved.

In an attempt to investigate whether the transverse acoustic field shortens the length of the jet or only bends it, a curved or total length was also measured. In this case, the same contour already used to measure the axial length is divided into a left and a right side (see Figure 3C). The total length is defined as the average of the left and right sides. Because the curves had a lot of small scale spatial features believed not to be significant to the computation of the total length, the right and left sides were smoothed by three methods: 1) simple averages in the x and y direction (5 points), 2) median filtering, and 3) median filtering followed by simple averages. The simple average was chosen because it smoothed out the small scale features mentioned above while preserving the shapes of the larger scale structures which is what we are interested in. Similarly in the case of filtering, even though the magnitude of the curved length changes, the trends with respect to MR and VR are preserved.

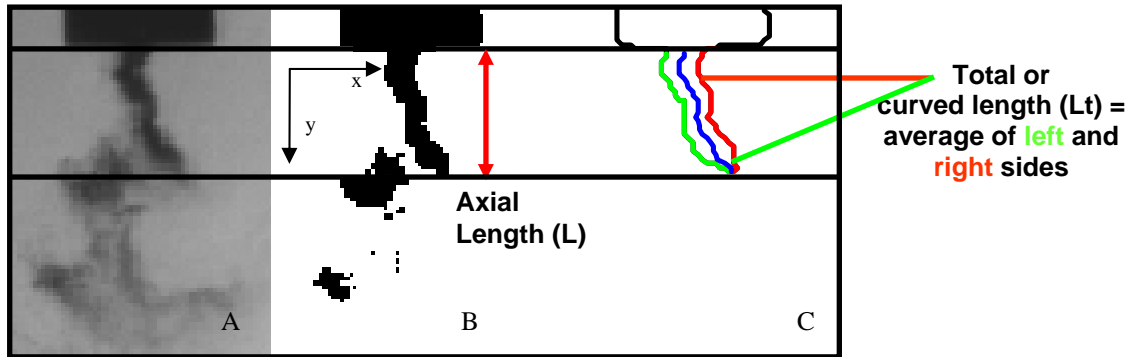


Figure 3. A. Raw image. B. Black and white image after thresholding showing definition of axial dark core length. C. Definition of total or curved length.

The lengths given by the Matlab subroutines were manually checked by selecting 50-60 images from each set of 2000 images and comparing the results with what the authors would select to be the length using the naked eye. Using these images the threshold level could be modified, if needed, from the one automatically computed and then used to process the complete set of images. In all cases, the axial and curved dark core lengths are normalized by the inner diameter of the inner jet ($D_1=0.51\text{mm}$)

A. Qualitative Characterization of Images

A collection of images taken at the three different chamber pressures is shown in Figs. 4-6. The first set of images (Fig. 4) corresponds to a subcritical pressure. For this case, the inner jet is a liquid with temperature of 109-110K and the outer jet is a gas with temperature from 175-195K. This is a two-phase mixture. The upper row of images has the acoustic field turned off. In the leftmost image the presence of droplets is evident, but as the VR and MR increase the dark core and the droplets become smaller and finally, for the conditions of the rightmost image, the droplets have become irresolvable by the pixel size of the image. This behavior is consistent with previous data^{7-8,11} where as MR and VR increase the mixing becomes more efficient between the two jets and the inner jet mixes faster with its surroundings. When the transverse acoustic field is turned on (lower row in Fig. 4) the jet also moves in the transverse direction. As will be shown later, the movement of the jet has the same frequency as the driving frequency of the piezo-siren. We can also intuitively see that the acoustics have the most effect on the jet, in terms of the decrease in axial dark core length and the amount of discernable bends, in a range of MR from about 1-4, which we will also confirm quantitatively later.

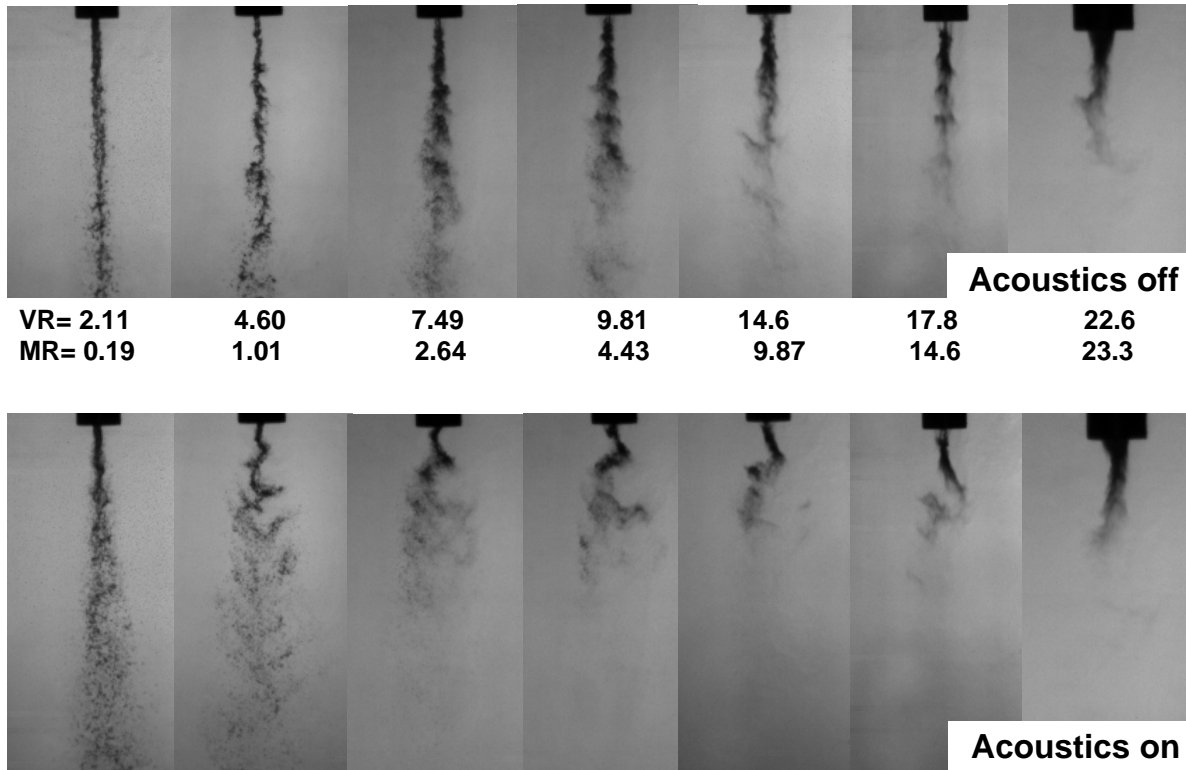


Figure 4. Collection of images at subcritical pressure (~1.5 MPa) with acoustics on and off for MR:0.19-23.3 and VR:2.11-22.6. The driving frequency is ~3kHz

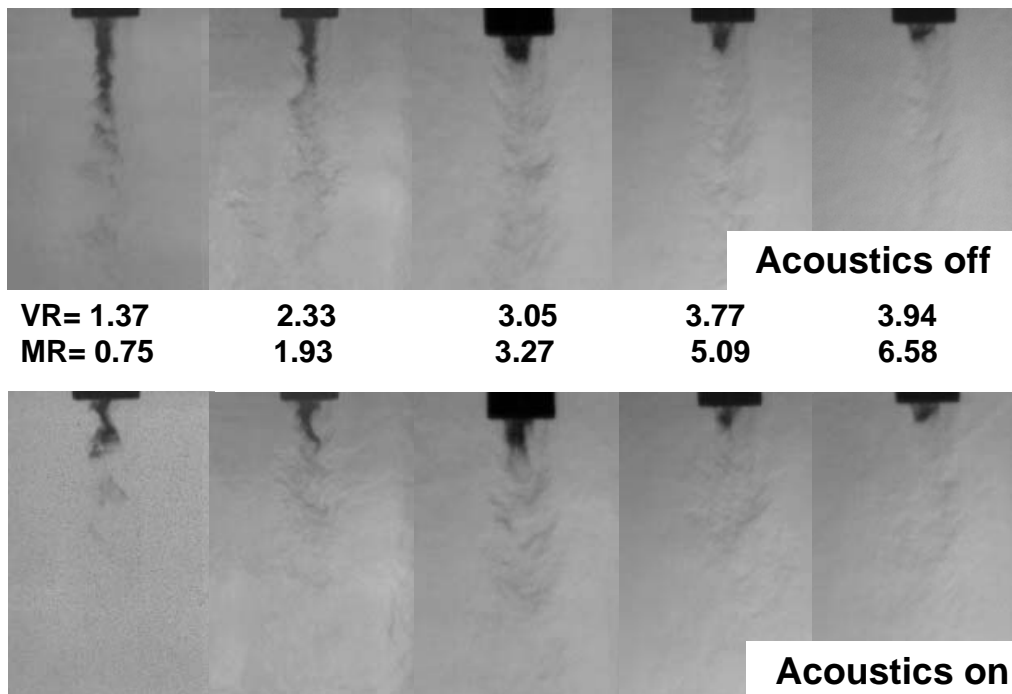


Figure 5. Collection of images at nearcritical pressures (~3.6 MPa) for acoustics on and off for MR:0.75-6.58 and VR:1.37-3.94. The driving frequency is ~3kHz.

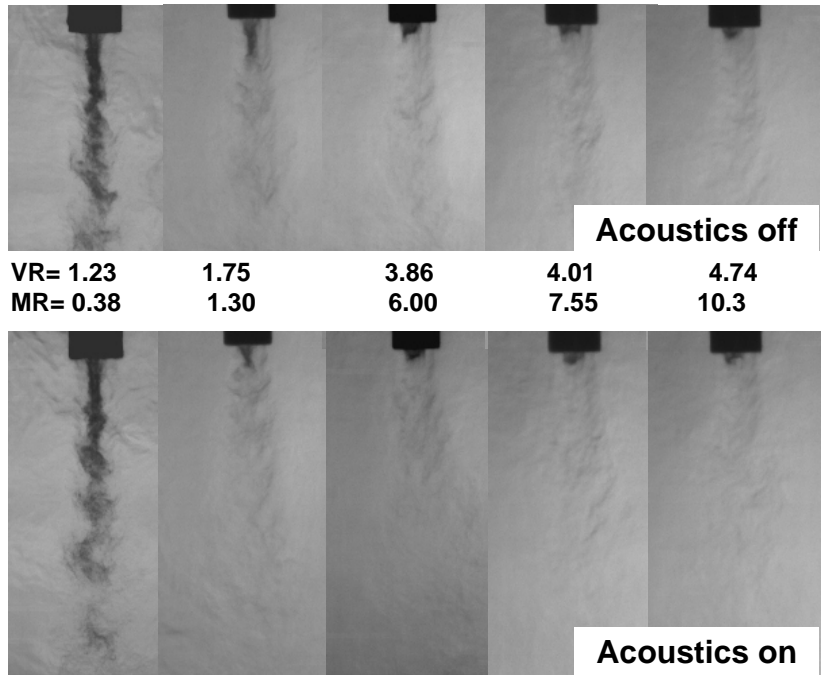


Figure 6. Collection of coaxial jet at supercritical pressure (~4.9 MPa) with acoustics on and off for MR: 0.38-10.3 and VR: 1.23-4.74. The driving frequency is ~3 kHz.

As the pressure increases to nearcritical values (Fig. 5) we notice some differences. In this case the inner jet is a few degrees above the critical temperature and the outer jet temperature varies from 171-195K. Both jets are in a supercritical state. This is a one-phase mixture. Notice that there are no more visible droplets in this situation, even for the low VR's, as we would expect since the inner jet is not a liquid anymore. At this pressure, the dark core length has become smaller for a given MR and VR due in part to the fact that the difference in temperatures between the two jets is smaller than for subcritical P's. By VR values of ~4, the length of the jet has become $< \sim 5 D_1$. In this case, when the acoustics are turned on, a dramatic shrinkage in the axial length is visible for the two leftmost images, but as the MR increases the changes become less

discernable and the bending of the jet becomes more of a straight motion of the short jets in the transverse direction. Similar observations apply for Fig. 6 which depicts jets at supercritical pressures and supercritical temperatures as well.

B. Axial Dark Core Length

Next, a quantitative characterization of the jet's response to the acoustic field is offered by plotting the axial dark core length as a function of MR. The results are shown in Fig. 7. This figure includes all the data gathered in this study. Solid symbols correspond to data with no acoustics and the corresponding hollow symbols denote data when the acoustics are on. The color codes and symbols are also applicable to the rest of the figures in this paper. The error bars denote $\pm 1\sigma$ (standard deviation). The two sets of blue data correspond to subcritical pressures. Within subcritical pressure data, the light blue or cyan corresponds to a set of data taken with a nearly constant outer jet temperature of 180-181K. This is done to compare with the other subcritical data to see if there is a direct effect of the outer jet temperature (besides its implicit effect through density and MR) on the dark core length. As the figure shows, these data blend well with the rest of the subcritical data which includes a broad range of outer jet temperatures from 112-195K. Therefore, there is no direct effect of the outer jet temperature on the axial dark core length within the range of MRs tested here. The other point to indicate has to do with the system repeatability in the subcritical regime. For a few conditions (namely around MR=1 and MR=5), run conditions were repeated within a few weeks to a couple of months. In all cases the variability is within the error bars of the test data.

The magenta diamonds correspond to nearcritical pressures with the inner jet at supercritical T while the magenta squares have inner jet temperatures below or within 1K of the critical T. The yellow data points are also at nearcritical pressures but the temperature of the inner jet is within 1K of the critical T while the outer jet temperatures are $> 180K$. Finally the red data corresponds to supercritical pressures. One of the most striking things from this figure is that there are two branches for the dark core length plotted versus MR. This new data confirms previous data gathered in this facility and other historical data^{7,11}.

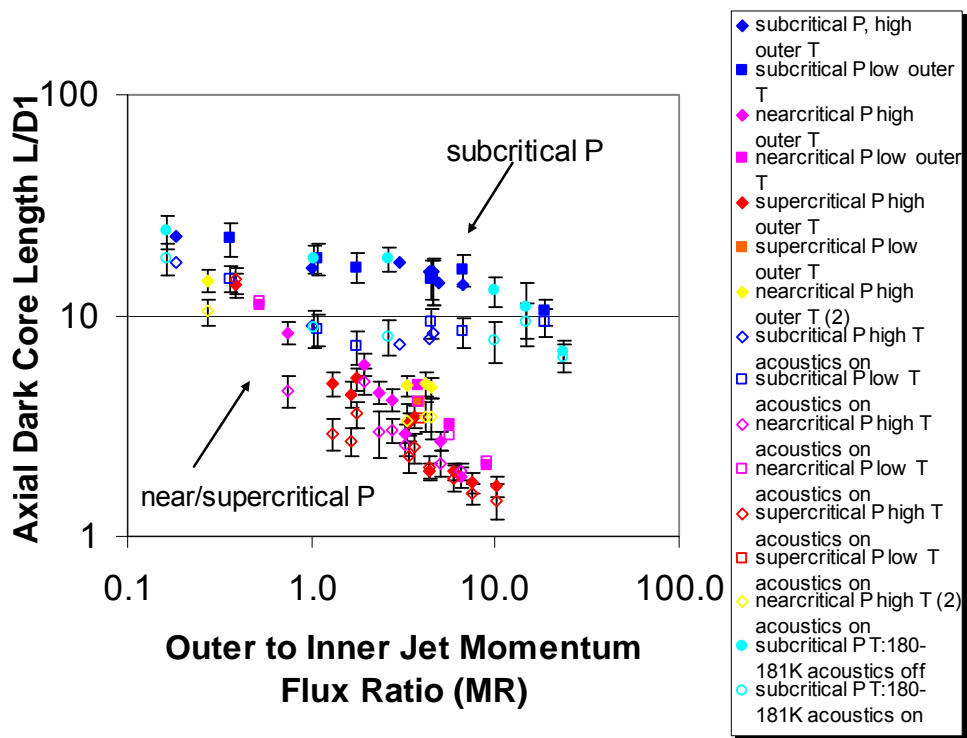


Figure 7. Variation of the axial dark core length as a function of MR for both acoustics on and off

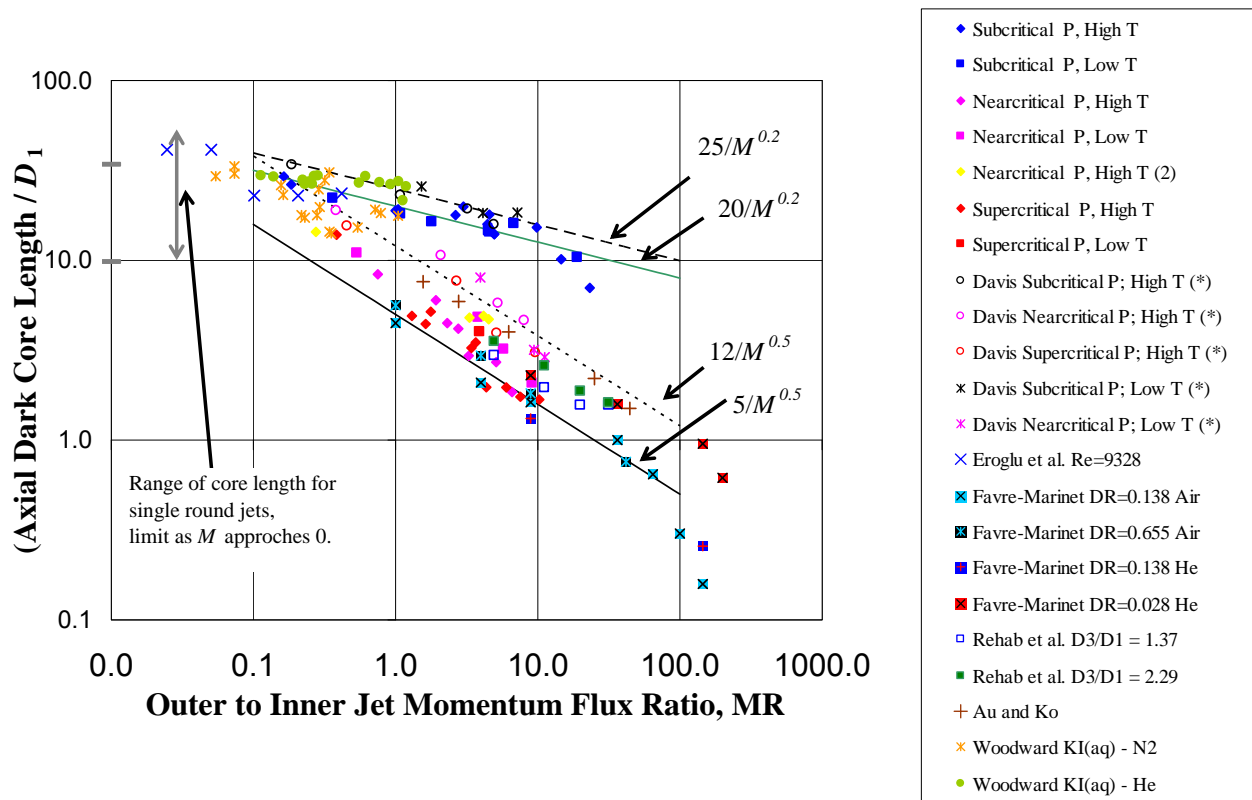


Figure 8. Summary of historical and current data on the trends of the axial dark core length vs. MR

In fact this was one of the objectives of the present study, to verify the trends of the axial dark core length vs. MR with more robust statistics due to the fact that the new runs have more data points per run than before and there are more points per pressure range. Also, note that differences in the axial dark core length for acoustics on and off are statistically significant for $\sim 1 < MR < \sim 4$ under all chamber pressures. This is especially clear for the subcritical pressures. Next, this data is plotted along with the previously gathered data from this facility and historical data by others^{7-8,11} (Fig. 8). In previous studies^{7,11} the trend for the single-phase mixtures (near and supercritical P) was shown to follow a functional relation of the form A/MR^n where n is 0.5 and A : [5-12] whereas for the two-phase mixtures (subcritical P) the exponent was 0.2 and A was 25. For the current data, although a least squares fit for near and supercritical P gives $7.3/MR^{0.58}$, all but one point (including error bars) are included in the previous bracket. Similarly for the subcritical data, a least square fit gives $18.4/MR^{0.19}$ but all the data except for one point (including error bars) are contained in $A/MR^{0.5}$ if A is 20-25.

A trend we wanted to examine with this study is the effect of VR on the standard deviation (std. dev.) of the axial dark core length. This is because preliminary data^{7-8,11} indicated that the std. dev. decreased with VR offering perhaps insight into why injectors for cryogenic liquid rocket engines designed for high VR provide more stable combustion than those working at lower VR's. That is, a lower std. dev. is indicative of the jet's insensitivity to externally imposed acoustics which would make it more "stable". Of course, this and the previous studies are performed with N_2 instead of combusting gases, and this hypothesis needs to be further verified using reacting mixtures. The results for the axial length std. dev. are presented in Fig. 9 for all the data gathered in this study. The general trend, with the exception of a few outliers, is the same as observed before. The std. dev. decreases with VR, and the magnitudes are lower for near and supercritical pressures. Two new observations can be made from this data set; the first is that the fastest drop in std. dev. values happens at low VR's. At around VR=5, the std. dev. decrease becomes more gentle. The second observation is that for subcritical pressures, the std. dev.'s of the cases with acoustics on are lower than their no-acoustics counterparts and follow the same trend. For the near and supercritical pressure cases no conclusions can be drawn as the differences in the std. dev. mostly fall within the pixel resolution for these images, which is $\sim 0.2D1$.

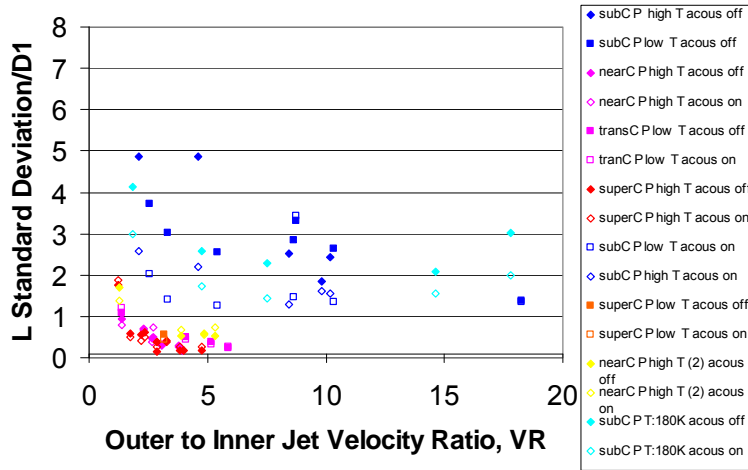


Figure 9. Standard deviation of the axial dark core length vs. VR

C. Curved or Total Dark Core Length

One of the questions that arose while conducting this study was whether the acoustics were indeed shortening the dark core or merely bending it. If the core is only being bent then we would expect the acoustics not to have much effect on mixing but if the core is being bent and shortened then acoustics are expected to have an impact on mixing. To answer this question, the definition of curved length described in Fig. 3 was employed. As mentioned previously, the curved lengths were smoothed by using a five point average around every point both in the x and y directions. Fig. 10 shows the results for the curved dark core length vs. MR. The data for these lengths with no smoothing was previously reported but the trends do not change¹². This figure is the counterpart to Fig. 7. One interesting observation is the great resemblance between both figures. Except for the fact that the lengths are larger

(as intuitively expected) all the observations made for Fig. 7 still apply. However, by virtue of Fig. 10 having curved as supposed to axial lengths, the fact that we see statistically significant differences between the cases with and without acoustics means that the jet is indeed shortened by the acoustic field when $\sim 1 < MR < \sim 4$. These differences are clearer in the curved dark core lengths. Finally, to conclude the comparison between the curved and axial dark core lengths, the std. dev. has been plotted against VR in Fig. 11. The data shows more scatter than those for the axial dark core length but the general trends are the same.

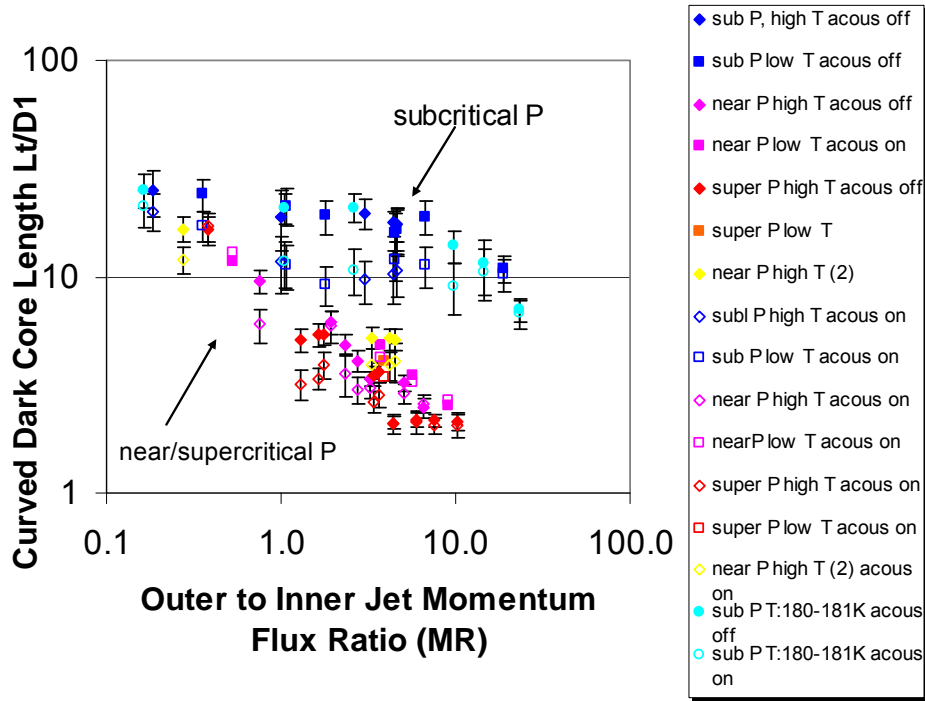


Figure 10. Trend of the Curved Dark Core Length vs. MR

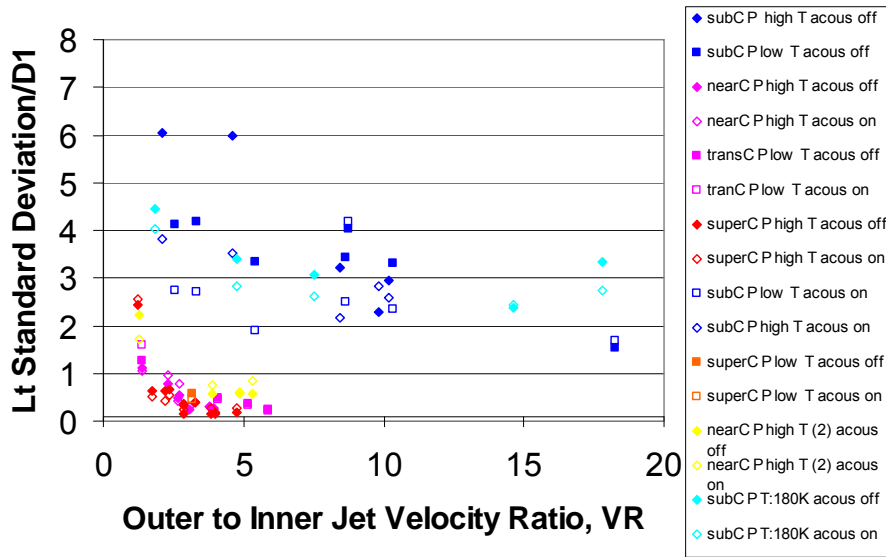


Figure 11. Standard Deviation of the Curved Dark Core Length vs. Velocity Ratio, VR

D. Frequency analysis

The last part of this paper is a preliminary presentation of the frequency analysis done on the transverse and axial movements of the dark core of the jet. Fig. 12 A&B shows a sample of the axial and curved lengths as a function of time for Run sb14 (Appendix) with acoustics on. In both cases, the dominant frequency is so prevalent that one can estimate it by merely counting the peaks. Also, note that the lengths have a saw tooth shape vs. the sinusoidal shape of the signal that is fed into the piezo-siren. Fig. 13 A&B show the FFT's of the axial and smooth curved lengths. The fundamental frequency in both cases is also about 3.043 kHz vs 3.06 kHz fed into the piezo-siren, which is a very good agreement (0.6% difference). Fig. 14 A shows a sample of the movement of the midpoint of the inner jet with time for the 10th row from the injector's exit plane. This row was chosen arbitrarily. The movement of the midpoint is evident in Fig. 14 B which shows two snapshots of the jet at about half a cycle apart highlighting the row examined. The FFT's of the width of the jet and the midpoint again at the 10th row from the injector's exit plane is shown in Fig. 14 C&D. We see that the main frequency is again 3.043kHz. Together, the movement of the inner jet's midpoint and width tell the story of the dynamics of the jet. Because the midpoint of the inner jet is moving, the peak in the width can be attributed to both the movement of the entire jet's width left and right and to its contraction and expansion. These preliminary results hint to the complex motion of the dark core of the jet in the transverse and axial directions when affected by a transverse acoustic field. A more detailed study of the frequency analysis of the behavior of the jet will be the subject of a future paper.

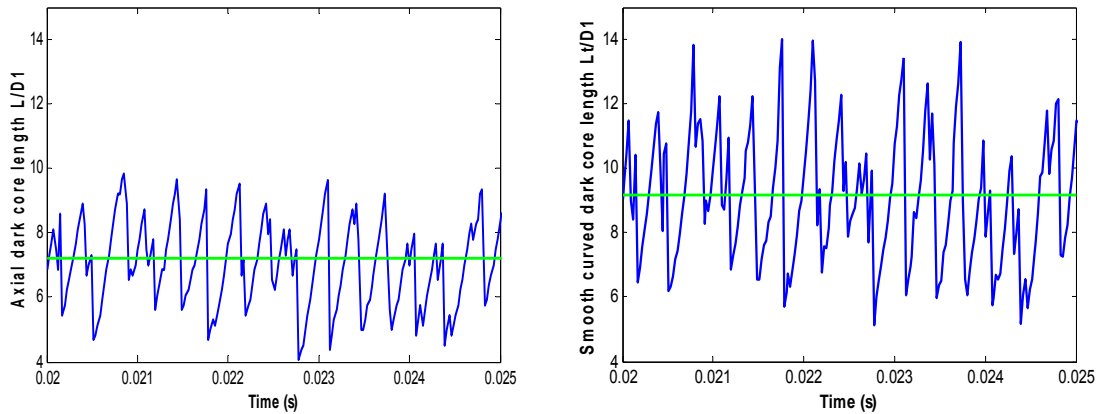


Figure 12. A. Time trace of axial dark core length. B. Time trace of curved dark core length.

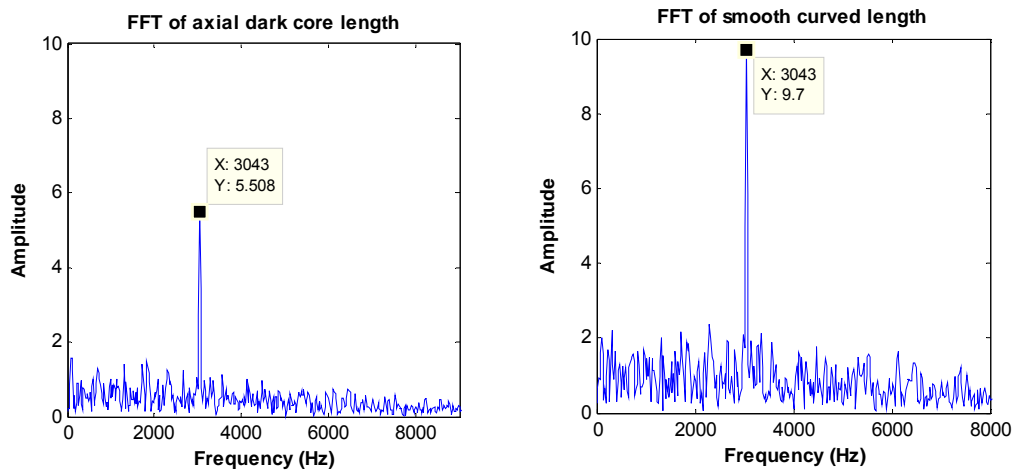


Figure 13. A. FFT of axial dark core length. B. FFT of curved dark core length

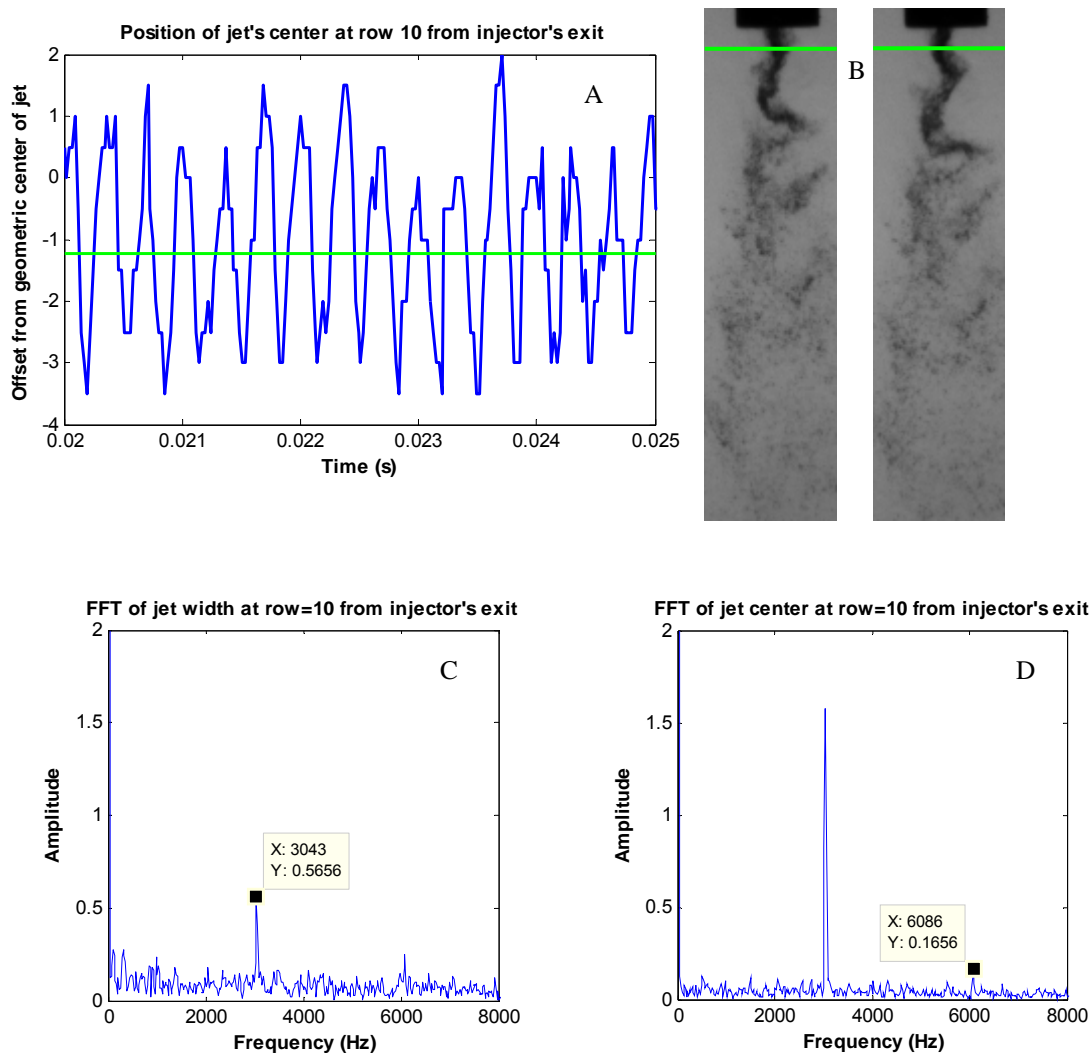


Figure 14. A. Sample of position of the inner jet's center with time at row 10 from injector's exit. B. Jet at two different times highlighting row 10 from injector's exit. C. FFT of jet width at row 10 from injector's exit. D. FFT of jet's center at row 10 from injector's exit.

V. Conclusion

An extensive study was carried out to characterize the effects of a transverse acoustic field on a coaxial jet spanning subcritical to supercritical chamber pressures. The main parameter used to assess the effects of the acoustics and operating conditions on the jet is the dark core length. Both the axial and the total, or curved, dark core lengths were investigated. In this study, at least 2000 images were taken at 41 kHz for each test condition giving more robust statistics such as the mean and the standard deviation of the dark core length than previously obtained (30 frames per condition at 10 Hz). The new data confirmed that the standard deviation of the axial dark core length decreases as VR increases. This trend was also observed in the curved or total dark core length

introduced in this paper. As the standard deviation decreases the jet becomes more insensitive to external fluctuations which can offer insight into why liquid rocket engine injectors designed to operate at $VR > \sim 10$ are more stable than those designed to operate at lower VR values. At subcritical pressures, the std. dev. of both lengths decreases when the acoustics are turned for a given MR and VR. For the near and supercritical pressure cases no conclusions can be drawn as the differences in the std. dev. mostly fall within the pixel resolution for these images. The current axial dark core length data falls within a band defined by $L = A/MR^n$, with the exponent being 0.2 (A:20-25) for subcritical pressures, and 0.5 (A:5-12) for near and supercritical pressures. With the exception of opening the band from A=20 to A:20-25 for subcritical pressures, the results agree with previous data.

A new key finding, resulting from the study of the total dark core length, is that for $\sim 1 < MR < \sim 4$, acoustics do shorten the dark core which implies that acoustics enhance mixing in this range. This answers the question of whether the acoustic field imposed on the jet only bends the jet or bends it and shortens it. For this range of MR's the differences in the curved lengths are larger than the error bars ($\pm\sigma$) in the data. This range is even larger for subcritical pressures. Outside this range the differences between the curved dark core length with and without acoustics fall within the statistical uncertainty of the measurements. Especially for $MR > \sim 4$ in the near and supercritical pressures, the core becomes small enough that the differences between acoustics on and off mostly fall within the resolution of the camera. Preliminary data is also presented to characterize the frequencies of the jet's movement in the transverse and axial directions. As one would expect, the frequency describing the transverse and axial movements of the jet is the same as the driving frequency of the acoustic field. Future work will include further characterization of the acoustic pressure field which will give a precise measurement of the acoustic pressure field for every test condition. Also, further frequency analysis of the jet, and variation of the position of the pressure and velocity nodes with respect to the jet center will be performed. This last part will allow us to see the effects not only of magnitude but also of gradient of the acoustic pressure and velocity on the jet's behavior.

Appendix

SUBCRITICAL PRESSURE											
HIGH OUTER JET TEMPERATURE											
	sb1	sb2	sb3	sb4	sb5	sb6	sb7	sb8	sb9	sb10	sb11
T chamber (K)	231	237	252	240	243	241	250	243	245	250	214
ρ chamber (kg/m ³)	22.4	21.1	19.9	21.1	21.0	20.8	20.3	20.9	20.6	20.1	24.0
P chamber (MPa)	1.51	1.46	1.47	1.49	1.49	1.47	1.49	1.49	1.48	1.48	1.49
P chamber (psia)	220	212	213	216	217	213	216	216	214	214	216
T outer (K)	181	195	175	180	181	195	184	189	181	181	184
\dot{m} outer (mg/s)	316	315	785	787	1270	1260	1620	1600	2410	2950	3680
ρ outer (kg/m ³)	29.6	26.2	29.8	29.2	29.2	26.4	28.6	27.5	28.8	28.8	28.5
u outer (m/s)	4.09	4.61	10.1	10.3	16.6	18.3	21.6	22.2	32.1	39.1	49.4
Re outer (x10 ³)	4.14	3.89	10.5	10.3	16.6	15.6	20.9	20.2	31.6	38.6	47.7
T inner (K)	110	109	110	109	110	110	110	110	110	110	110
\dot{m} inner (mg/s)	281	281	280	280	282	278	280	278	279	280	279
ρ inner (kg/m ³)	625	629	626	629	621	625	621	624	623	623	626
u inner (m/s)	2.21	2.21	2.21	2.20	2.24	2.19	2.22	2.20	2.21	2.22	2.20
Re inner (x10 ³)	12.4	12.3	12.4	12.2	12.7	12.3	12.6	12.4	12.5	12.6	12.4
VR	1.86	2.11	4.60	4.73	7.49	8.43	9.81	10.2	14.6	17.8	22.6
MR	0.164	0.185	1.01	1.04	2.64	3.00	4.43	4.59	9.87	14.6	23.3
Acoustics Off											
L/d1	24.0	22.7	16.5	18.1	18.2	17.5	15.9	15.7	12.9	10.9	6.89
L _T /d1	25.1	24.8	19.0	20.9	20.9	19.6	17.7	17.4	13.8	11.5	7.06
Acoustics On											
Frequency (kHz)	2.97	2.95	2.99	2.97	2.97	2.97	2.99	2.97	2.97	3.00	3.03
L/d1	18.2	17.4	8.90	8.79	8.05	7.47	7.86	8.28	7.71	9.31	6.43
L _T /d1	21.0	20.1	11.8	11.7	10.8	9.65	10.3	10.6	9.03	10.5	6.77

	SUBCRITICAL PRESSURE							NEARCRITICAL PRESSURE			
	LOW OUTER JET TEMPERATURE										
	sb12	sb13	sb14	sb15	sb16	sb17	sb18	nr12	nr13	nr14	nr15
T chamber (K)	233	221	228	234	213	213	213	216	210	215	209
ρ chamber (kg/m ³)	21.5	23.3	22.1	21.5	23.9	24.2	24.1	58.7	60.3	58.7	60.5
P chamber (MPa)	1.46	1.49	1.48	1.47	1.47	1.50	1.48	3.57	3.54	3.54	3.54
P chamber (psia)	212	217	214	213	214	217	215	517	513	514	513
T outer (K)	157	112	146	148	148	144	154	138	143	157	141
\dot{m} outer (mg/s)	504	1170	1170	1860	1860	2320	3690	1410	3450	4040	5650
ρ outer (kg/m ³)	33.9	61.0	37.8	37.1	37.1	39.1	35.2	130	115	94.3	121
u outer (m/s)	5.69	7.36	11.9	19.1	19.2	22.7	40.1	4.14	11.5	16.4	17.8
Re outer (x10 ³)	7.36	21.7	18.1	28.5	28.5	36.3	54.6	19.1	47.0	53.6	77.0
T inner (K)	109	110	110	110	110	110	110	125	123	126	125
\dot{m} inner (mg/s)	284	281	279	281	279	278	280	291	292	286	287
ρ inner (kg/m ³)	628	619	625	623	621	619	624	482	508	442	465
u inner (m/s)	2.23	2.24	2.20	2.23	2.21	2.22	2.21	2.98	2.84	3.19	3.05
Re inner (x10 ³)	12.4	12.8	12.4	12.6	12.6	12.7	12.5	22.0	20.2	24.9	23.1
VR	2.58	3.31	5.43	8.66	8.74	10.3	18.3	1.40	4.09	5.17	5.89
MR	0.358	1.08	1.78	4.47	4.55	6.73	18.8	0.530	3.77	5.72	9.06
Acoustics Off											
L/d1	22.3	18.2	16.5	14.7	14.5	16.1	10.4	11.1	4.85	3.23	2.09
L _T /d1	24.1	21.2	19.1	16.0	16.6	19.0	10.9	11.7	4.80	3.50	2.52
Acoustics On											
Frequency (kHz)	2.96	3.04	3.06	3.07	3.05	3.04	3.02	3.12	3.11	3.13	3.13
L/d1	14.7	8.72	7.21	9.32	14.5	8.43	9.37	11.6	4.09	2.85	2.18
L _T /d1	17.1	11.3	9.17	12.1	16.6	11.2	10.2	13.0	4.19	3.22	2.68

NEARCRITICAL PRESSURE – HIGH OUTER JET TEMPERATURE											
	ABOVE CRITICAL TEMPERATURE INNER JET							NEAR CRITICAL TEMP. INNER JET			
	nr1	nr2	nr3	nr4	nr5	nr6	nr7	nr8	nr9	nr10	nr11
T chamber (K)	254	228	251	251	234	247	238	237	232	236	230
ρ chamber (kg/m ³)	47.6	54.8	49.2	48.8	53.1	49.8	51.9	51.7	52.5	54.3	53.6
P chamber (MPa)	3.52	3.56	3.58	3.54	3.56	3.55	3.54	3.53	3.56	3.55	3.56
P chamber (psia)	510	517	518	514	516	515	514	511	517	515	516
T outer (K)	194	179	179	186	171	192	195	182	189	184	194
\dot{m} outer (mg/s)	2030	3070	3130	3850	3950	4950	6120	802	3140	3140	3130
ρ outer (kg/m ³)	66.4	75.5	75.9	70.9	80.8	68.0	66.7	72.9	69.7	72.6	67.2
u outer (m/s)	11.7	15.5	15.8	20.8	18.7	27.9	35.1	4.21	16.51	17.8	17.22
Re outer (x10 ³)	23.8	37.9	38.7	46.4	50.1	58.5	71.8	9.81	38.2	36.8	37.4
T inner (K)	130	128	128	129	128	129	132	126	127	127	126
\dot{m} inner (mg/s)	289	290	289	290	288	287	286	287	288	288	288
ρ inner (kg/m ³)	167	213	244	182	230	190	157	422	319	416	420
u inner (m/s)	8.56	6.72	5.84	7.88	6.18	7.44	8.97	3.35	3.43	3.38	4.52
Re inner (x10 ³)	58.2	52.1	47.5	56.4	49.4	54.6	58.5	26.7	27.5	26.9	38.2
VR	1.37	2.33	2.72	2.66	3.05	3.77	3.94	1.26	3.89	4.88	5.32
MR	0.751	1.93	2.31	2.76	3.27	5.09	6.59	0.28	3.31	4.15	4.52
Acoustics Off											
L/d1	8.39	6.00	4.47	4.17	2.94	2.71	1.85	14.7	4.80	4.89	4.69
L _T /d1	9.48	6.14	4.86	4.07	3.35	3.23	2.47	16.6	5.23	5.17	5.10
Acoustics On											
Frequency (kHz)	3.00	2.99	3.05	3.05	3.01	3.06	3.05	3.06	3.01	3.02	3.00
L/d1	4.57	5.06	2.99	3.00	2.60	2.15	1.97	10.4	3.33	3.49	3.50
L _T /d1	6.00	5.91	3.57	3.01	3.05	2.87	2.58	12.0	3.88	3.88	4.06

SUPERCritical PRESSURE											
HIGH OUTER JET TEMPERATURE											LOW T
	sp1	sp2	sp3	sp4	sp5	sp6	sp7	sp8	sp9	sp10	sp11
T chamber (K)	240	251	241	245	234	232	236	225	236	227	209
ρ chamber (kg/m ³)	73.1	68.3	71.6	70.2	74.4	75.2	73.8	78.7	72.9	77.1	86.7
P chamber (MPa)	5.00	4.93	4.93	4.93	4.94	4.92	4.94	4.95	4.89	4.93	4.96
P chamber (psia)	725	715	715	714	716	714	716	718	709	715	719
T outer (K)	184	176	173	172	175	185	195	183	188	191	150
\dot{m} outer (mg/s)	1170	2800	2780	2810	4550	4240	5750	5810	7050	8140	4620
ρ outer (kg/m ³)	106	113	117	118	115	104	95.7	107	100	99.0	165
u outer (m/s)	4.23	9.46	9.09	9.10	15.2	15.7	23.0	20.9	26.9	31.5	10.7
Re outer (x10 ³)	13.5	32.9	32.9	33.3	53.6	48.8	64.6	67.3	80.9	92.5	54.6
T inner (K)	132	137	134	133	137	136	147	138	141	141	132
\dot{m} inner (mg/s)	293	294	291	293	296	295	295	292	293	293	294
ρ inner (kg/m ³)	416	266	342	373	271	302	179	264	214	216	423
u inner (m/s)	3.47	5.45	4.20	3.88	5.38	4.83	8.12	5.45	6.76	6.69	3.42
Re inner (x10 ³)	27.5	43.7	34.7	31.7	43.4	39.7	53.4	43.6	49.8	49.4	26.9
VR	1.23	1.75	2.18	2.36	2.85	3.27	2.86	3.86	4.01	4.74	3.15
MR	0.384	1.30	1.63	1.77	3.42	3.66	4.35	6.00	7.55	10.3	3.87
Acoustics Off											
L/d1	13.9	4.91	4.42	5.18	3.25	3.49	1.97	1.96	1.74	1.68	4.03
L _T /d1	16.4	5.12	5.35	5.45	3.46	3.64	2.11	2.17	2.17	2.12	4.08
Acoustics On											
Frequency (kHz)	3.10	3.11	3.29	3.26	3.26	3.22	3.08	3.19	3.08	3.05	3.10
L/d1	10.2	2.92	2.70	3.58	2.32	2.54	2.05	1.84	1.55	1.45	3.40
L _T /d1	12.2	3.18	3.38	3.92	2.65	2.85	2.09	2.12	2.06	2.06	3.45

Acknowledgments

The authors would like to recognize Randy Harvey for his invaluable contributions on running and maintaining the facility. Also thanks to Juan Rodriguez for preparing the appendix. This work is sponsored by AFOSR under Mitat Birkan, program manager.

References

1. Oswald, M., Smith, J. J., Branam, R., Hussong, J., Schik, A., Chehroudi, B., Talley, D., "Injection of Fluids into Supercritical Environments", *Combustion Science and Technology*, Vol. 178, No. 1-3, 2006, pp. 49-100.
2. Culick F. E. and Yang, V., "Overview of Combustion Instabilities in Liquid-Propellant Rocket Engines," *Liquid Rocket Engine Combustion Instability*, edited by V. Yang and W. Anderson, Progress in Astronautics and Aeronautics, AIAA, Washington, DC, 1995, pp. 3-38.
3. Muss, J., Chakroborty, S., Leyva, I. A., "Development of the Scorpion LOX/Kerosene engine family", *JANNAF 2005-0356*, 2nd Liquid Propulsion and 1st Spacecraft Propulsion Subcommittee Meeting, Monterey, California, December 5-8, 2005.
4. Marshall, W., Pal, S., Woodward, R., Santoro, R. J., Smith, R., Xia, G., Sankaran, V., Merkle, C. L., "Experimental and Computational Investigation of Combustor Acoustics and Instabilities, Part II: Transverse Modes"; *AIAA 2006-538*

5. Yang, V., Anderson W., editors, *Liquid Rocket Engine Combustion Instability*, Progress in Astronautics and Aeronautics, Vol. 169, 1995
6. Sutton, G. P., *Rocket Propulsion Elements*, Sixth Edition, John Wiley & Sons, Inc., NY, 1992
7. Davis, D. W., Chehroudi, B., "Measurements in an acoustically driven coaxial jet under sub-, near-, and supercritical conditions", *JPP*, Vol. 23, No. 2, March- April 2007
8. Davis, D. W., Chehroudi, B., Sorensen, I., "Measurements in an acoustically driven coaxial jet under supercritical conditions", *AIAA 2005-736*
9. REFPROP, Reference Fluid Thermodynamic and Transport Properties, Software Package, Ver. 7.0, NIST, U.S. Department of Commerce, Gaithersburg, MD, 2002.
10. Otsu, N., "A threshold selection method from gray-level histograms", *IEEE transactions on Systems, Man, and Cybernetics*, Vol. 9, No. 1, 1979, pp. 62-66.
11. Davis, D., "On the behavior of a shear-coaxial jet, spanning sub- to supercritical pressures, with and without an externally imposed transverse acoustic field", Ph.D. Thesis, Dept. of Mechanical Engineering, Penn State University, 2005.
12. Leyva, I. A., Chehroudi, B., Talley, D., "Dark-core analysis of Coaxial Injectors at Sub-, Near-, and Supercritical Conditions in a Transverse Acoustic Field", *54th JANNAF Meeting*, Denver, CO, May 14-18, 2007.